Journal of Catalysis **182,** 37–47 (1999)
Article ID jcat.1998.2311, available online at http://www.idealibrary.com on IDEAL®

Non-Faradaic Electrochemical Modification of Catalytic Activity

12. Propylene Oxidation on Pt

Anthony Kaloyannis and Constantinos G. Vayenas

Department of Chemical Engineering, University of Patras, GR-26500 Patras, Greece

Received April 13, 1998; revised October 19, 1998; accepted October 20, 1998

The rate of complete propylene oxidation on polycrystalline Pt films deposited on 8 mol% Y_2O_3-stabilized-ZrO_2 (YSZ), an O^{2-} conductor, can be reversibly enhanced by up to a factor of 6 by varying the potential of the Pt catalyst film. The reaction rate increase is typically 2000 times higher than the electrochemically controlled rate of oxygen removal from the Pt catalyst surface. Electrochemical supply of promoting oxide ions does not affect significantly the catalytic rate. The catalytic reaction activation energy varies linearly by a factor of 4 with varying catalyst potential, leading to the appearance of the compensation effect. The observed pronounced promotional phenomena are discussed in view of the reaction mechanism, previous electrochemical promotion studies, and recent TPD and XPS investigations.

INTRODUCTION

During the last 9 years the effect of non-Faradaic electrochemical modification of catalytic activity (NEMCA) (1–3), or electrochemical promotion (4) or *in-situ* controlled promotion (5) has been studied in detail for over 50 catalytic reactions on Pt, Pd, Rh, Au, Ag, Ni, and IrO_2 catalysts using a variety of solid electrolytes including yttria-stabilized-zirconia (YSZ) (1–3), an O^{2-} conductor, β''-Al_2O_3 (5, 6), a Na^+ conductor, $CsHSO_4$ (7), $CaZr_{0.9}In_{0.1}O_{3-a}$ (8) and Nafion (9), H^+ conductors, CaF_2 (10), a F^- conductor, and TiO_2 (11), a mixed ionic–electronic conductor as the active catalyst support. The phenomenon has also been recently described in aqueous electrolyte systems (12–14). Work in this area has been reviewed extensively (15–17).

The porous metal or metallic oxide (18) catalyst film acts simultaneously as an electrode in a galvanic cell of the type

Gaseous reactants, metal catalyst | solid electrolyte | metal, O_2

and the NEMCA effect is induced by applying currents or potentials (typically -2 to $+2V$) between the catalyst and the metal counter electrode. By using YSZ as the solid electrolyte the observed induced increase in catalytic rate is up to 3×10^5 times higher than the rate, $I/2F$, of O^{2-} supply to the catalyst (2, 15–17) (where I stands for the applied current and F for Faraday's constant) and up to 100 times higher than the catalytic rate when no current is applied (19).

Three parameters are commonly used for the investigation and macroscopic description of electrochemical promotion:

(1) The enhancement factor or Faradaic efficiency, Λ, defined by

$$\Lambda \equiv \Delta r/(I/2F), \qquad [1]$$

where Δr is the induced change in catalytic rate expressed in mol O/s. The current, I, is defined positive when anions are supplied to the catalyst. A catalytic reaction exhibits the NEMCA effect when $|\Lambda| > 1$. When $\Lambda > 1$ the reaction is termed electrophobic, while when $\Lambda < -1$ the reaction is termed electrophilic. As shown both experimentally (15–17) and theoretically (15–17) the order of magnitude of the absolute value, $|\Lambda|$, of the Faradaic efficiency Λ can be estimated for any reaction, catalyst, or solid electrolyte from

$$|\Lambda| \approx 2Fr_o/I_o \qquad [2]$$

where r_o is the open-circuit (unpromoted) catalytic rate and I_o is the exchange current of the electrocatalytic (charge-transfer) reaction at the catalyst-solid electrolyte interface. It is apparent from Eq. [2] that in order to obtain a non-Faradaic rate enhancement ($|\Lambda| > 1$) it is necessary to have a catalytic reaction intrinsically faster than the corresponding electrocatalytic reaction, i.e. $r_o > (I_o/2F)$.

(2) The rate enhancement ratio ρ, defined by

$$\rho = r/r_o. \qquad [3]$$

(3) The promotion index P_i of the promoting ion i defined by

$$P_i = \frac{\Delta r/r_o}{\Delta\theta_i}, \qquad [4]$$

0021-9517/99 $30.00

where θ_i is the coverage of the promoting species (e.g., $O^{\delta-}$, $Na^{\delta+}$) on the catalyst surface. When the promoting species does not react significantly with any of the reactants (e.g., $Na^{\delta+}$) then its coverage on the catalyst surface can be calculated accurately via coulometry (5, 6); P_{Na} values up to 3000 have been measured for the NO reduction by H_2 on Pt (20). However, when the promoting species (e.g., $O^{\delta-}$) is also partially consumed by one of the reactants then the P_i computation is less accurate. In such cases an approximate P_i estimation can be obtained from $P_i = (\Delta r/r_o)_{max}$, i.e. by assuming that the maximum rate enhancement is obtained for $\Delta\theta_{O^{\delta-}} = 1$ (16, 21). A more precise method for calculating $\theta_{O^{\delta-}}$, and thus $P_{O^{\delta-}}$, has been described recently (22).

Recent XPS (21, 23–24), SERS (25, 26), cyclic voltammetric (27), TPD (27), and STM (28) investigations have provided strong evidence that the NEMCA effect is due to an electrochemically controlled migration (back-spillover) of ionic species from the solid electrolyte onto the gas-exposed catalyst-electrode surface, as originally proposed on the basis of rate transients (2, 15). These backspillover ionic species change the catalyst surface work function, $e\Phi$, by

$$\Delta(e\Phi) = e\Delta V_{WR}, \qquad [5]$$

where V_{WR} is the catalyst (working electrode, W) potential relative to the reference (R) electrode (3, 29, 30). Consequently electrochemical promotion is due to the promoting action of these backspillover species ($O^{\delta-}$ in the case of YSZ, $Na^{\delta+}$ in the case of β''-Al_2O_3) which influence the chemisorptive bond strength of reactants and intermediates via through-the-metal and through-the-vacuum interactions (15–17). Recent *ab initio* quantum mechanical calculations using model metal clusters with oxygen atoms coadsorbed with ions or point charges have been used to explore the effect of work function on oxygen adsorption (31). It was shown that the binding strength of oxygen decreases significantly with increasing work function (31).

The nature of the promoting $O^{\delta-}$ species on Pt interfaced with YSZ has been investigated with XPS (21), SERS (25), cyclic voltammetry (27), and TPD (27). The XPS investigation has shown that its O 1s binding energy is at 528.8 eV (21). The TPD investigation has shown that its peak desorption temperature is at $T_p \approx 750$–780 K vs $T_p \approx 675$–685 K for weakly bonded atomic oxygen (O 1s binding energy at 530 eV (21)) which coexists on the Pt surface and is shifted to this weakly bonded state from its normal chemisorptive state ($T_p \approx 720$–730 K) by the coadsorbed strongly bonded $O^{\delta-}$ species (27).

The complete (32–38) and partial (39–44) oxidation of propylene has been studied on various metal oxide (39–44) and metal (32–38) surfaces including Pt (32–38). Salmeron and Somorjai (45) have investigated propylene desorption and decomposition on the Pt(111) crystal face and found that the first step for propylene decomposition is the abstraction of one hydrogen atom which results to the formation of a propylidyne species ($\equiv CCH_2CH_3$). Propylene adsorption on Pt(111) has been studied in detail by Anderson, Kang, and Kim (46) who found that propylene adsorption is favoured via di-σ coordination with the C=C double bond parallel to the surface and that bonding to the surface is a result of propylene π-orbital stabilization due to mixing with Pt s-d band orbitals (donation interaction) and Pt band stabilization due to mixing with the higher lying empty π^*-orbital (back-bonding interaction). They also found as Salmeron and Somorjai (45) that the initial decomposition step is the α-hydrogen abstraction which leads to the formation of propylidyne via 1,2-hydrogen shifts in the allyl species.

In this work we study the electrochemical promotion effect for propylene oxidation on polycrystalline Pt deposited on YSZ. Similarly with the cases of CO oxidation on Pt/YSZ (15, 16) and Ag/YSZ (15, 16) and of C_2H_6 oxidation on Pt/YSZ (22), propylene oxidation is found to exhibit a pronounced electrophilic NEMCA enhancement with negative currents, i.e., atomic oxygen removal from the catalyst surface. Positive current application, i.e., $O^{\delta-}$ supply to the catalyst, does not influence the reaction rate.

EXPERIMENTAL

The atmospheric pressure continuous flow apparatus has been described previously (6, 11, 15, 19, 47). Reactants were Messer Griesheim certified standards of C_3H_6 in He and O_2 in He. They could be further diluted in ultrapure (99.999%) He. Reactants and products were analyzed by on-line gas chromatography using a Perkin-Elmer Sigma 300 gas chromatograph with a TC detector and a Perkin-Elmer LCI-100 computing integrator. A Porapak Q column was used to separate O_2, C_3H_6, CO_2, and H_2O. No other products were detected. The CO_2 concentration in the reactor effluent was also continuously monitored using an Anarad Infrared CO_2 analyzer. Most of the kinetic experiments were carried out with a total volumetric flowrate of 400 cm^3 STP/min.

The well-mixed quartz reactor of volume 30 cm^3 was of the single-pellet type (48, 49); i.e., the YSZ disc (19-mm diameter, 2-mm thickness) was suspended in the quartz tube (Fig. 1a) with three Au wires attached to the catalyst, counter, and reference electrodes.

The Pt catalyst film (mass 0.2 mg, superficial surface area 0.78 cm^2) was deposited on one side of the YSZ disc using a thin coating of unfluxed Engelhard A1121 Pt paste followed by drying and calcination in air, first for 2 h at 400°C, then for 2 h at 900°C (Fig. 1b). The true surface area of the Pt film was obtained by measuring its reactive oxygen uptake at 350°C using the isothermal titration technique; the Pt film is exposed to O_2 for several min and then the reactor is purged with ultrapure He for a time t_{He}, several times

longer than the reactor residence time to remove gaseous O_2. Subsequently the reactor is purged with C_2H_4 and the amount of oxygen, N, remaining on the surface is measured by integrating the area of the reactor effluent CO_2 peak. By varying t_{He} one can study the oxygen desorption kinetics (15–17). Extrapolation of N to $t_{He}=0$ gives the reactive oxygen catalyst uptake N_O. Figure 2 shows the results of the surface titration measurements. The reactive oxygen uptake is $N_O=6.8\times10^{-7}$ mol O.

Gold counter and reference electrodes were deposited on the other side of the disc using thin coatings of Au paste prepared from a slurry of Au powder (Aldrich Chemicals) in ethyl acetate, followed by drying and calcination, first at 400°C for 2 h, then at 950°C for 2 h. Au was chosen as the auxiliary electrode material because of its inertness for C_3H_6 oxidation, as checked via blank experiments, which makes it an adequate (±0.1 *V*) oxygen pseudoreference electrode when using the single pellet design, as discussed elsewhere (50).

RESULTS

Open-Circuit Kinetics

Figures 3 and 4 show the rate dependence of propylene oxidation, r, on oxygen and propylene partial pressures, P_{O_2} and $P_{C_3H_6}$, respectively under open circuit, i.e. unpromoted, conditions. In these and subsequent figures the propylene oxidation rate is expressed in mol O/s and also as turnover frequency (TOF), i.e. oxygen atoms reacting per surface site per s, by using the reactive oxygen uptake, $N_O=6.8\times10^{-7}$ mol O, of the Pt catalyst film.

As shown in Fig. 3 the rate is positive-order in oxygen under oxygen-lean conditions and zero order under oxygen-rich ones over the entire temperature range investigated in this work. Figure 4 shows that the rate exhibits a sharp maximum with respect to propylene pressure at a $P_{C_3H_6}$ value, hereafter denoted $P^*_{C_3H_6}$, which is weakly dependent on temperature. The kinetics depicted in Figs. 3 and 4 suggest a competitive adsorption mechanism of dissociatively chemisorbed oxygen and propylene (45) with stronger binding of propylene than oxygen on the catalyst surface, which leads to the appearance of the rate maximum at $P^*_{C_3H_6}$.

Promotional Transients

Figure 5 shows a typical galvanostatic transient; i.e., it depicts the catalytic rate and catalyst potential response upon current application.

At $t=0$ the circuit is open ($I=0$) and the steady state (unpromoted) catalytic rate is 3.58×10^{-7} mol O/s. Upon negative current application ($I=-65\,\mu$A corresponding to the steady-state removal of $I/2F=3.37\times10^{-10}$ mol O/s) the rate increases by a factor of 3.5. The rate increase $\Delta r=8.92\times10^{-7}$ mol O/s is 2648 times larger than the rate

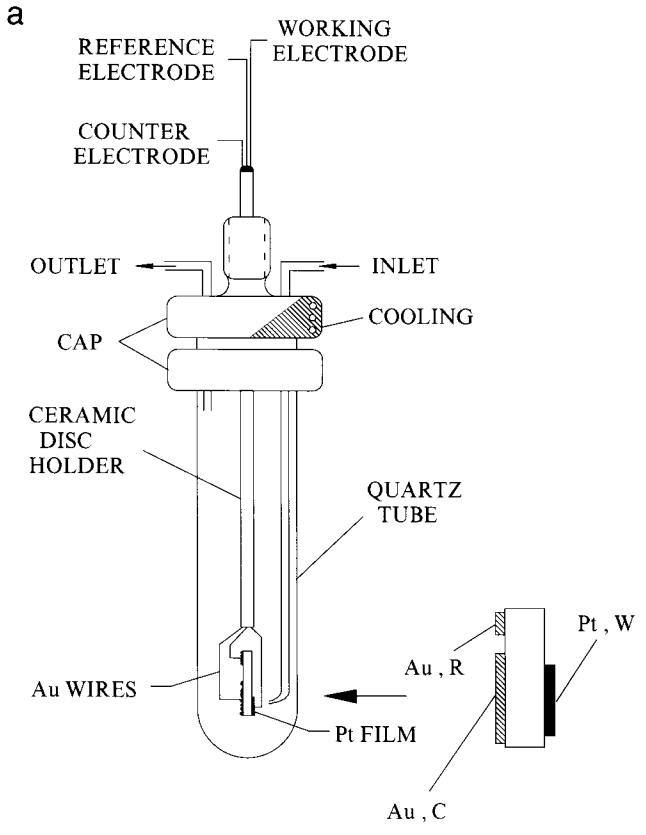

FIG. 1. (a) Single pellet catalytic reactor and three-electrode configuration; (b) scanning electron micrographs of the Pt catalyst-electrode.

($-I/2F$) of oxygen removal. This implies that each O^{2-} removed from the catalyst causes, on the average, 2648 chemisorbed oxygen atoms to react with propylene and form CO_2 and H_2O. Consequently for the galvanostatic transient of Fig. 5 the enhancement factor, or Faradaic efficiency, Λ, and rate enhancement ratio, ρ, equal -2648 and 3.5, respectively:

$$\Lambda=\Delta r/(I/2F)=-2648 \quad [6]$$

$$\rho=r/r_0=3.5. \quad [7]$$

The negative sign in the Faradaic efficiency, Λ, value shows that the reaction exhibits electrophilic behavior (15, 17) upon negative current application, i.e.

$$\Lambda<0,\quad \partial r/\partial V_{WR}<0,\quad P_{O_{2-}}<0. \quad [8]$$

Positive current application was not found to have a measurable effect on the catalytic rate. It is worth noting in Fig. 5 that the time required for the rate to reach steady state after constant current application is of the order of $2FN/I$, which is the time required for the removal of a monolayer of atomic oxygen from the catalyst surface. This observation has been made in practically all previous NEMCA studies (16, 17) and has provided the first evidence that NEMCA is

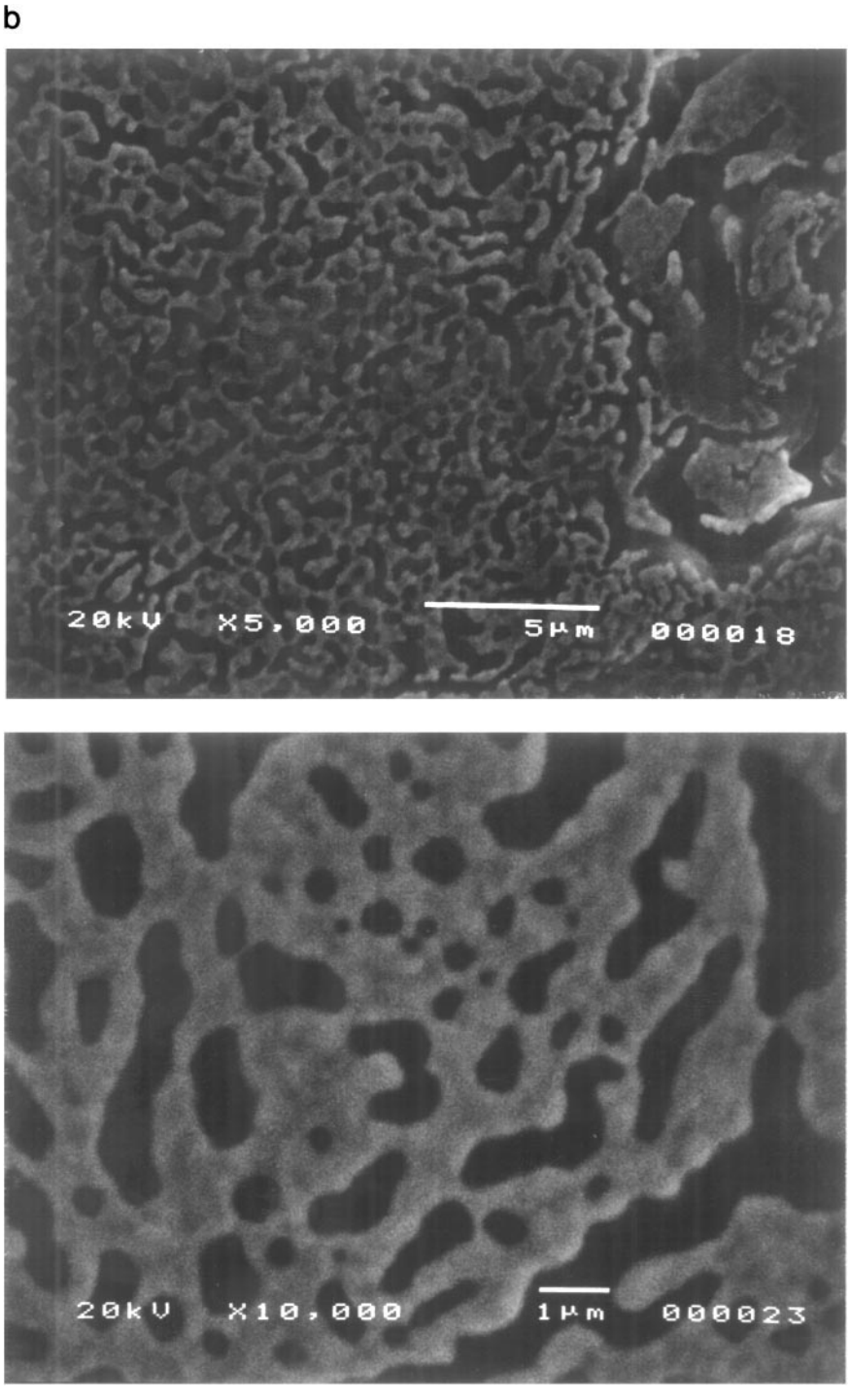

FIG. 1—*Continued*

due to electrochemically controlled spillover/backspillover of ionic species between the catalyst and the supporting solid electrolyte.

Electrocatalytic Kinetics

Figure 6 shows the dependence of the current, I, on catalyst overpotential η. The latter is defined from

$$\eta = V_{WR} - V^{o}_{WR}, \quad [9]$$

where V^{o}_{WR} is the open-circuit ($I = 0$) catalyst potential. It is apparent that the current-overpotential behaviour is symmetrical for anodic ($I > 0$) and cathodic ($I < 0$) currents and, thus, can be described by a single value of the exchange current I_o in the Butler–Volmer equation:

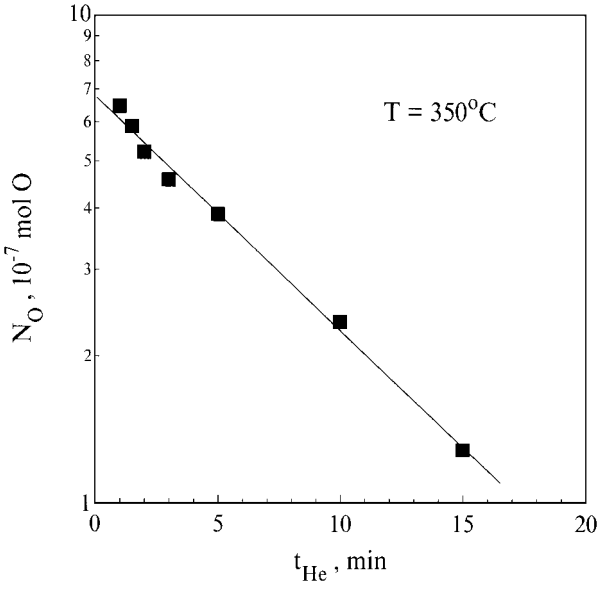

FIG. 2. Isothermal titration of surface oxygen with C_2H_4; the effect of oxygen desorption time, t_{He}, on the mass of reactive oxygen on the Pt catalyst surface.

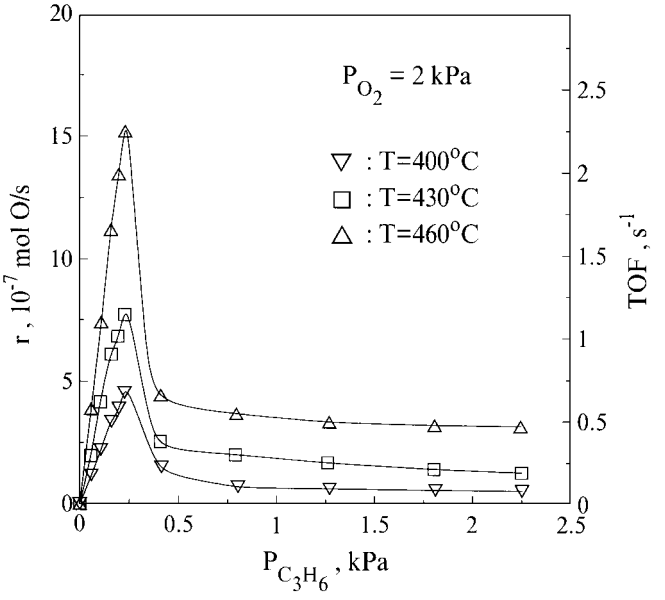

FIG. 4. Effect of $P_{C_3H_6}$ and temperature on the rate and turnover frequency of propylene oxidation.

$$\ln(I/I_o) = \alpha_\alpha F\eta/RT - \alpha_c F\eta/RT. \quad [10]$$

This shows that the adsorbed species coverages do not change appreciably with the catalyst potential (15–17).

For intermediate $|\eta|$ values the Butler–Volmer equation reduces to the Tafel Equations,

$$\ln(I/I_{o,\alpha}) = \alpha_\alpha F\eta/RT, \quad [11]$$

$$\ln(I/I_{o,c}) = \alpha_c F\eta/RT, \quad [12]$$

for anodic and cathodic operation, respectively. In these equations $I_{o,\alpha}$, $I_{o,c}$, and α_α, α_c are the apparent anodic and cathodic excange currents and transfer coefficients, respectively.

For low $|\eta|$ values the Butler–Volmer equation reduces to

$$I/I_o = (\alpha_\alpha + \alpha_c)F\eta/RT. \quad [13]$$

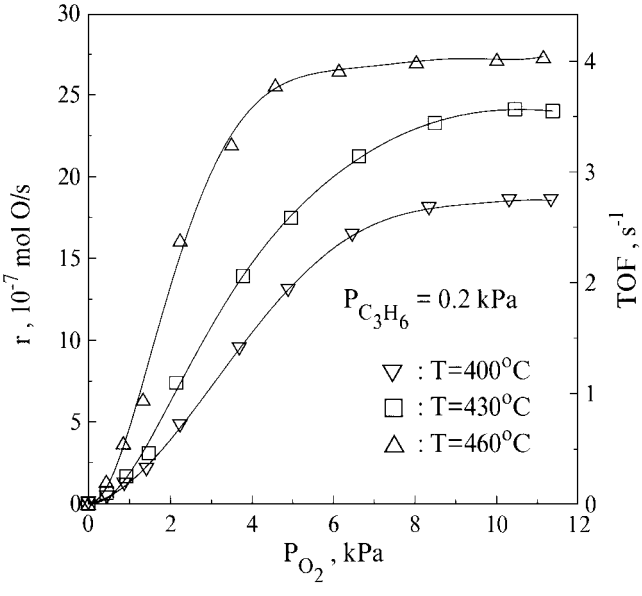

FIG. 3. Effect of P_{O_2} and temperature on the rate and turnover frequency of propylene oxidation.

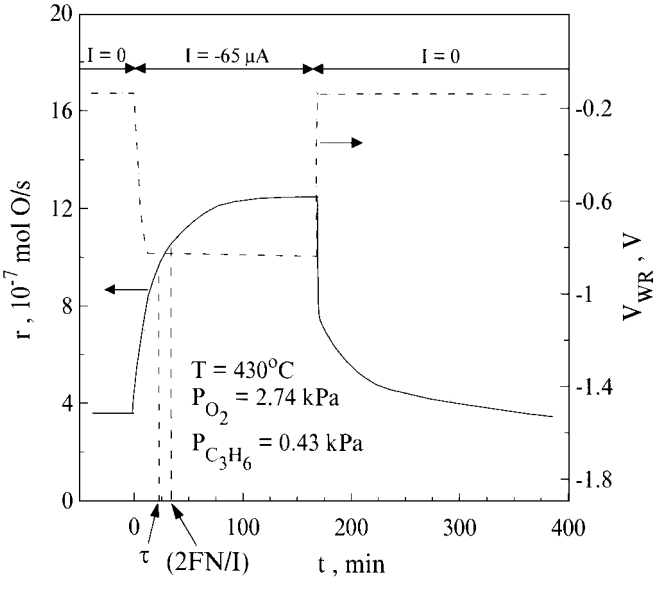

FIG. 5. Electrochemical promotion: propylene oxidation rate (continuous line) and catalyst potential (dashed line) response to step changes in applied negative current. See text for discussion; $r_o = 3.58 \times 10^{-7}$ mol O/s, $P_{O_2} = 2.74$ kPa, $P_{C_3H_6} = 0.43$ kPa, $N = 6.79 \times 10^{-7}$ mol O.

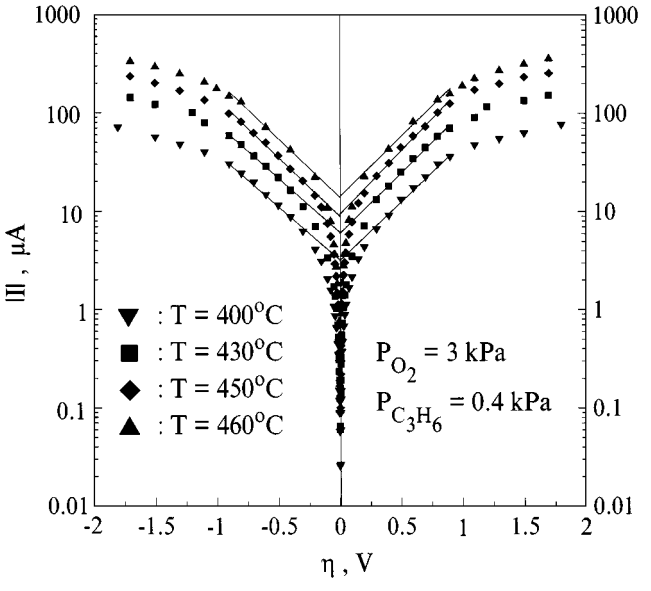

FIG. 6. Effect of catalyst overpotential $\eta(=V_{WR}-V^{o}_{WR})$ on the cell current.

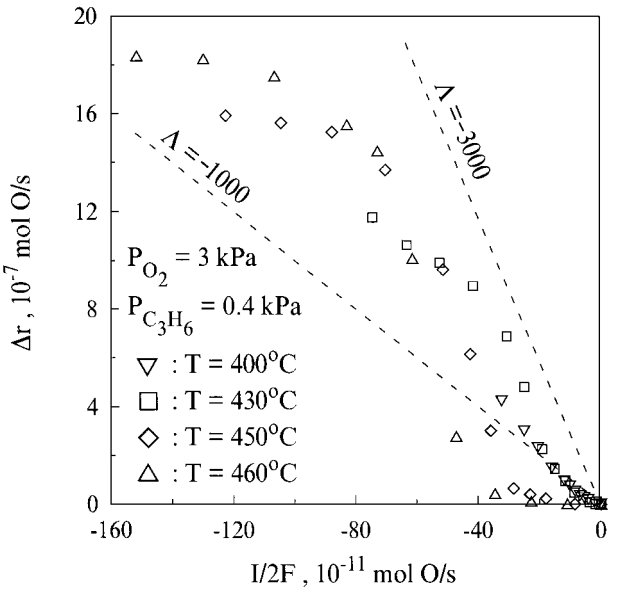

FIG. 7. Effect of the rate, $I/2F$, of electrochemical oxygen ion removal ($I<0$) on the induced increase in the rate of C_3H_6 oxidation.

Calculating α_a and α_c from Eqs. [11], [12] and substituting their values in Eq. [13] we determine the I_o value. Table 1 lists the extracted $I_{o,\alpha}$, $I_{o,c}$, α_α, α_c, and I_o values. Comparison of $I_{o,\alpha}$, $I_{o,c}$ with I_o shows that their values are very close; Also $I_{o,\alpha}$, $I_{o,c}$ and I_o increase exponentially with temperature with an apparent activation energy equal to 27 kcal/mol, while both α_α and α_c remain practically constant and equal to 0.25.

Steady-State Effect of Current on the Catalytic Rate

Figure 7 shows the steady-state effect of applied current, I, on the increase in the propylene oxidation rate. As shown in this figure the enhancement factor, or Faradaic efficiency, Λ, takes values between -1000 and -3000. The measured $|\Lambda|$ values deviate significantly from those predicted by the approximate relationship:

$$|\Lambda| \approx 2Fr_o/I_o \qquad [2]$$

as also shown in Table 1. It is worth noting, however, that despite this significant deviation, the measured Λ values show the same qualitative trends with the parameter $2Fr_o/I_o$; i.e., $|\Lambda|$ is larger at lower temperatures, where I_o is significantly smaller (Table 1).

TABLE 1

Electrokinetic Parameters and Open-Circuit Catalytic Rate

$T/^\circ$C	$I_{o,a}/\mu$A	$I_{o,c}/\mu$A	I_o/μA	α_a	α_c	$r_o/(10^{-7}$ mol O/s)	$2Fr_o/I_o$
400	3.17	3.24	2.81	0.16	0.14	2.62	18000
430	5.99	6.16	6.04	0.17	0.15	3.36	10730
450	9.38	8.98	8.78	0.18	0.17	3.81	8380
460	14.19	14.04	15.69	0.18	0.17	4.04	4970

Note. $P_{O_2}=3$ kPa; $P_{C_3H_6}=0.4$ kPa.

Effect of Catalyst Potential

Figure 8, based on the data of Figs. 6 and 7, shows the catalytic rate dependence on catalyst potential V_{WR} or, equivalently (3, 29, 30), catalyst work function change $\Delta(e\Phi)$.

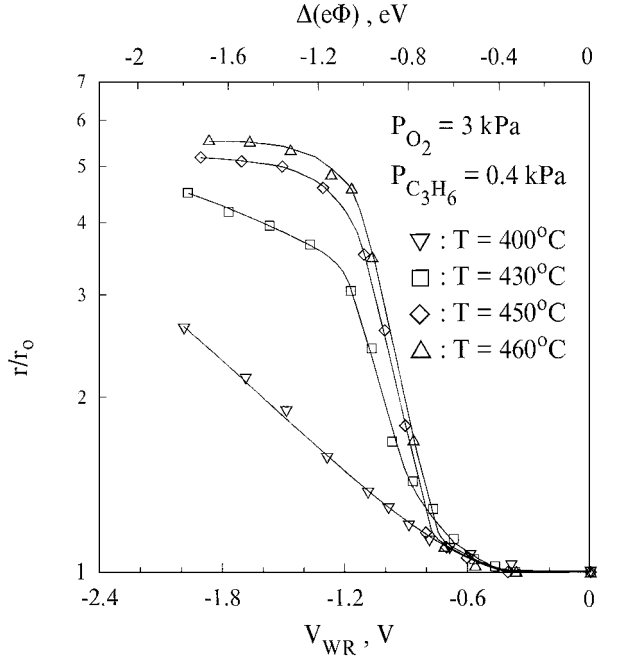

FIG. 8. Effect of catalyst potential and work function change on the rate enhancement ratio $\rho(=r/r_o)$ at fixed gaseous composition. The open-circuit rate, r_o, equals 2.62×10^{-7} mol O/s, 3.36×10^{-7} mol O/s, 3.81×10^{-7} mol O/s, and 4.04×10^{-7} mol O/s at $T=400^\circ$C, 430°C, 450°C, and 460°C, respectively.

For negative potentials the reaction exhibits electrophilic behavior and in the range $-1.2\ V < V_{WR} < -0.7\ V$ the rate increases exponentially with decreasing catalyst potential and work function according to

$$\ln(r/r_o) = \alpha(e\Phi - e\Phi^*)/k_bT, \qquad [14]$$

where k_b is Boltzmann's constant. The parameter α, termed the NEMCA coefficient (15–17), is of the order of -0.22 in this region except for $T = 400^\circ$C, where its absolute value is of the order of 0.05. This exponential-type rate dependence on the catalyst potential and work function is a common observation in numerous previous NEMCA studies (15–17).

The positive potential region is not depicted on this figure because, as previously noted, application of a positive current (or potential) does not have a measurable effect on the catalytic rate.

Comparison of Figs. 6 and 8 leads to the observation that the ranges of potential, or overpotential, where there is an exponential rate versus potential relationship (Eq. [14]) coincide to a large extent with the ranges where the exponential current versus potential dependence is valid.

Figure 9 shows the effect of catalyst potential V_{WR} on the reaction kinetics with respect to oxygen. Two observations can be made: (a) Negative potentials significantly decrease the P_{O_2} value, where the rate reaches a plateau. This observation suggests that decreasing V_{WR} and catalyst work function $e\Phi$ strengthen the chemisorptive bond of oxygen as in previous electrochemical promotion studies of catalytic oxidation reactions (15–17). (b) Negative potentials enhance the rate only for low P_{O_2} values. Under such low $P_{O_2}/P_{C_3H_6}$ values the rate is zero order in propylene (Fig. 4).

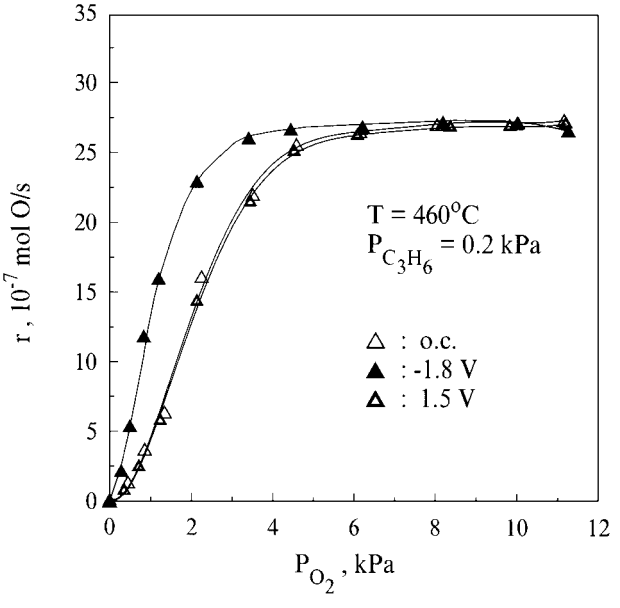

FIG. 9. Effect of P_{O_2} on the rate of C_3H_6 oxidation under open-circuit (o.c.) conditions and at various imposed catalyst potentials.

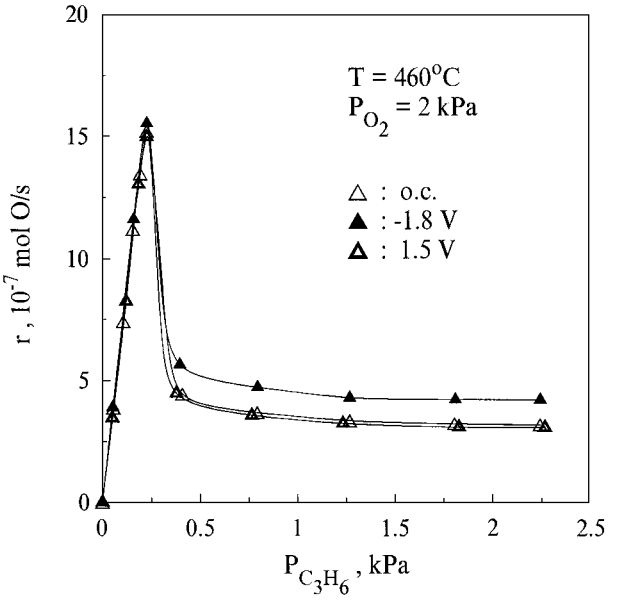

FIG. 10. Effect of $P_{C_3H_6}$ on the rate of C_3H_6 oxidation under open-circuit (o.c.) conditions and at various imposed catalyst potentials.

Figure 10 shows the effect of catalyst potential V_{WR} on the reaction kinetics with respect to propylene. It is worth noting that: (a) Negative potentials enhance slightly the rate only for high $P_{C_3H_6}$ values. Under such $P_{C_3H_6}/P_{O_2}$ values the rate is positive order in oxygen (Fig. 3). (b) The $P_{C_3H_6}$ value at the rate maximum remains unaffected with decreasing V_{WR}. Figures 9 and 10 show clearly that positive potentials do not affect the catalytic rate.

Effect of the Catalyst Potential on the Catalytic Activation Energy

Figure 11 shows Arrhenius plots obtained at various fixed values of catalyst potential and compare them with the open-circuit (o.c.) Arrhenius plot. Compensation effect behaviour is observed (51, 52). All Arrhenius lines corresponding to fixed potentials converge to a single isokinetic point, $T_\Theta = 653$ K.

Figure 12 shows the dependence of the apparent activation energy values, E, extracted from the Arrhenius plots of Fig. 11, on the catalyst potential V_{WR}. In the electrophilic region ($\partial r/\partial V_{WR} < 0$) depicted on this figure, the activation energy E decreases linearly with V_{WR} (and $e\Phi$) with a slope $\alpha_H = -0.9$:

$$\Delta E = \alpha_H \Delta(e\Phi). \qquad [15]$$

The apparent preexponential factor r^o; defined from

$$r = r^o \exp(-E/k_bT) \qquad [16]$$

follows the activation energy behaviour (Fig. 12). Its logarithm varies linearly with V_{WR} and, in fact, when plotted

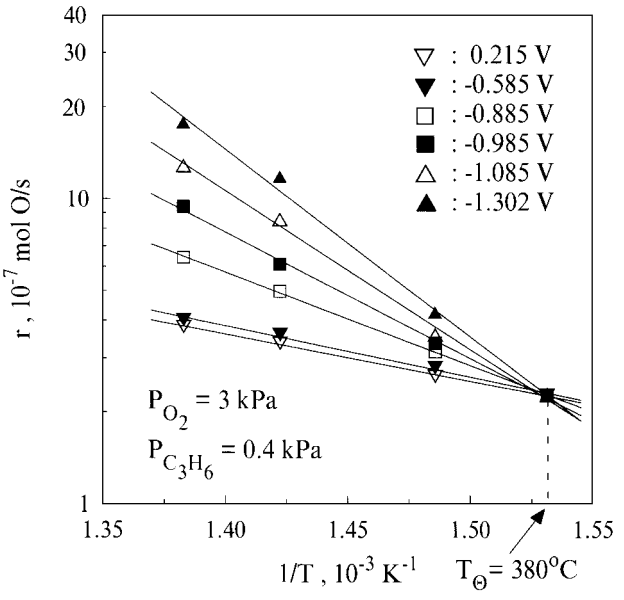

FIG. 11. Promotionally induced compensation effect: Arrhenius plots at various fixed negative catalyst potentials; comparison with the open-circuit (o.c.) Arrhenius plot.

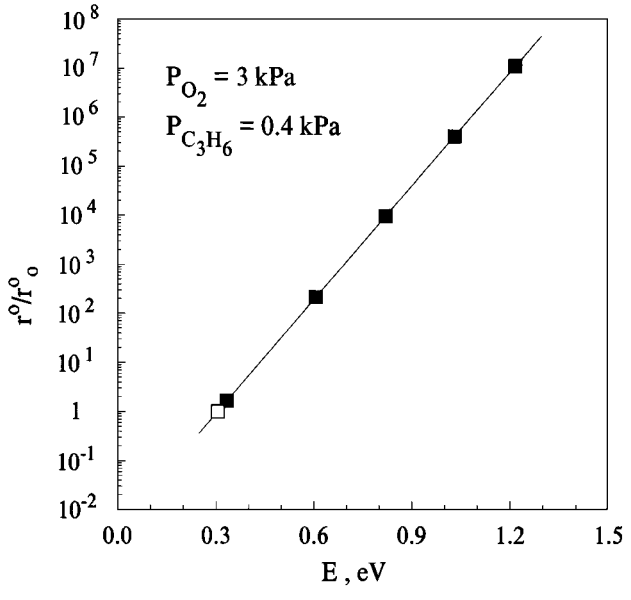

FIG. 13. Effect of the apparent activation energy, E, on the apparent preexponential factor r^o at various fixed negative potentials open symbol corresponds to open-circuit conditions.

as $k_b T_\Theta \ln(r_o/r_o^o)$, where T_Θ is the isokinetic point temperature and r_o^o is the open circuit preexponential factor, one obtains the same functional dependence on V_{WR}, displaced vertically by the open-circuit activation energy E_o (Fig. 12).

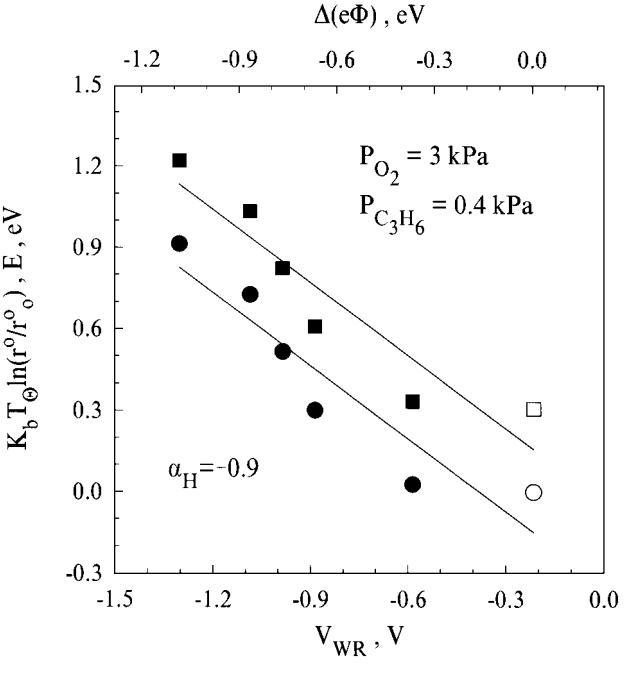

FIG. 12. Effect of catalyst potential and work function on the apparent activation energy E and on the logarithm of the preexponential factor r^o; r_o^o is the open-circuit preexponential factor and T_Θ is the isokinetic point temperature.

This happens because, as discussed previously (19), when an isokinetic point T_Θ exists, then E and $\ln r^o$ are related via

$$E - E_o = k_b T_\Theta \ln\left(r_o/r_o^o\right). \qquad [17]$$

Equation [17] is satisfied for each V_{WR} value and consequently when $\ln(r_o/r_o^o)$ is plotted versus E one straight line is obtained with slope $k_b T_\Theta$, as shown in Fig. 13.

DISCUSSION

The present work shows that the catalytic activity of Pt for propylene oxidation can be markedly affected via the NEMCA effect by using Y_2O_3-stabilized zirconia-ZrO_2 (YSZ) as an active catalyst support. In contrast to the case of C_2H_4 oxidation on Pt/YSZ (2), Pt/β''-Al_2O_3 (4), and Rh/YSZ (19), and also of C_2H_6 oxidation on Pt/YSZ (22), where the reaction is strongly electrophobic at high potentials, i.e. the rate increases significantly with O^{2-} supply to the catalyst; in the present case the reaction is unaffected under similar conditions.

Interestingly, propylene oxidation is found to exhibit a rather strong electrophilic behaviour ($\rho \approx 6$) at low potentials, i.e. with electrochemical removal of oxygen from the Pt surface. It is apparent that this type of electrophilic electrochemical promotion, also observed in the cases of CO oxidation on Pt/YSZ (15, 16) and Ag/YSZ (15, 16) and of C_2H_6 oxidation on Pt/YSZ (22), is not due to oxide ion backspillover, since oxygen is in this case being removed electrochemically from the Pt surface.

The observed compensation effect (50, 51) shows, in conjunction with other recent similar results (15–17), that the promotion-induced compensation effect is a rather common phenomenon, resulting from the linear variation of activation energy and the logarithm of preexponential factor with catalyst potential and work function (Fig. 12).

Origin of the Promoting Action

As previously mentioned it is now well established that when using YSZ and positive currents, the NEMCA effect is due to the promotional action of backspillover oxide ions O^{2-} (O 1s binding energy at 528.8 eV (21) peak desorption temperature $T_P \approx 750$–780 K (27)) which spread over the entire catalyst surface, increase its work function by

$$\Delta(e\Phi) = e\Delta V_{WR} \qquad [5]$$

and act as sacrificial promoters by reacting with chemisorbed oxidizable species at a rate Λ times smaller than the oxidation rate due to the displaced (27) more weakly bonded atomic oxygen ($T_P \approx 675$–685 K).

It is worth noting that Eq. [5] is also valid when applying negative currents, i.e. in the low catalyst potential region as well. Also the Helmholtz equation is valid in both regions (15–17),

$$e\Delta V_{WR} = \Delta(e\Phi) = -\frac{eN_m}{\varepsilon_o}\sum_j \Delta(P_{o,j}\cdot\theta_j), \qquad [18]$$

where N_m is the surface metal atom concentration (e.g. 1.53×10^{19} atom/m^2 for Pt(111)), $e = 1.6\times10^{-19}$ C/atom, $\varepsilon_o = 8.85\times10^{-12}$ C^2/J · m, and $P_{o,j}$ corresponds to the (average) dipole moment of each species j present on the catalyst surface at a coverage θ_j. Upon applying positive currents the increase in $e\Phi$ is obtained primarily by the increase in the coverage of the backspillover oxide ions $O^{\delta-}$ whose dipole moment is expected to be higher than that of other covalently bonded species (e.g., coadsorbed atomic oxygen and propylene). However, changes in the coverages and dipole moments of these coadsorbed species are also quite possible, as actually shown in TPD studies of oxygen on Pt/YSZ (27), where significant alterations in the chemisorptive state of coadsorbed atomic oxygen was observed (28).

When using negative currents in the Pt/YSZ system, no backspillover oxide migration to the catalyst surface can take place, only chemisorbed oxygen removal, and thus the Helmholtz equation [18] has to be accomodated only by changes in the coverages and dipole moments of dissociatively chemisorbed oxygen and propylene. A decrease in oxygen coverage will in general cause a decrease in $e\Phi$ (15–17) and a concomitant strengthening in the Pt=O chemisorptive bond. As depicted in Fig. 9 negative potentials cause a decrease in the P_{O_2} value where the reaction rate reaches a plateau ($P^*_{O_2}$), thus a strengthening of the Pt=O bond, as expected to be the case for electron acceptor adsorbates, such as atomic oxygen, upon decreasing the catalyst work function (15–17). Consequently one can attribute the electrochemical promotional action in the region of negative currents (and low potentials) to Eq. [5] in conjuction with the Helmholtz equation [18], i.e. to the fact that a decrease in potential leads to a decreased coverage and tighter binding of dissociatively chemisorbed oxygen (15–17) with a concomitant readjustment in surface coverages of oxygen and C_3H_6 in order to satisfy Eq. [5].

In this way one can rationalize the observed promotional features on the reaction kinetics with respect to P_{O_2} (Fig. 9) and $P_{C_3H_6}$ (Fig. 10) in terms of the following simple rule used to explain previous NEMCA studies. Decreasing catalyst work function via readjustment in surface coverages and dipole moments due to the applied potential, causes a strengthening in the chemisorptive bond strength of dissociatively chemisorbed oxygen (electron acceptor). This causes the decrease in $P^*_{O_2}$ (Fig. 9) with decreasing V_{WR} and $e\Phi$. In view of the fact that the dissociative C_3H_6 chemisorption on Pt involves both donation and backdonation of electrons (45, 46) it is not clear whether C_3H_6 chemisorption is strengthened or weakened with decreasing $e\Phi$. The overall effect appears to be small, in view of the observed insensitivity of the $P_{C_3H_6}$ value which maximizes the rate, $P^*_{C_3H_6}$, with changing potential (Fig. 10).

Activation Energy Dependence on Work Function and Compensation Effect

On the basis of the detailed analysis for a bimolecular catalytic reaction

$$A + B \rightarrow C + D, \qquad [19]$$

following Langmuir–Hinshelwood kinetics; i.e.,

$$r = k_R k_A k_B P_A P_B/(1 + k_A P_A + k_B P_B)^2 \qquad [20]$$

presented in the case of ethane oxidation on Pt/YSZ (22), the apparent activation energy of propylene oxidation reaction is given by

$$E = E_R + \frac{k_O P_{O_2}^{1/2} - k_{C_3H_6} P_{C_3H_6}}{k_O P_{O_2}^{1/2} + k_{C_3H_6} P_{C_3H_6}} \times \left[Q^o_O - Q^o_{C_3H_6} - (\alpha_1+\alpha_2)\Delta(e\Phi)\right], \qquad [21]$$

where E_R is the true activation energy, k_{O_2} and $k_{C_3H_6}$ are the adsorption equilibrium constants of O_2 and C_3H_6 and Q^o_O, $Q^o_{C_3H_6}$ are the corresponding heats of adsorption of O_2 and C_3H_6 under open-circuit conditions. The parameters α_1, α_2 ($\alpha_1 > 0$) express the variation, assumed linear (22, 31) of the heats of adsorption of O_2 and C_3H_6, respectively, with varying work function (22, 31).

From Eq. [21] it becomes apparent that the sign of $\partial E/\partial(e\Phi)$ depends on the sign of the parameter $A =$

$k_O P_{O_2}^{1/2} - k_{C_3H_6} P_{C_3H_6}$. For negative $\Delta(e\Phi)$ values oxygen adsorption is strong, relative to propylene adsorption; thus A is positive and, according to Eq. [21], E increases linearly with decreasing $\Delta(e\Phi)$. As in the case of C_2H_6 oxidation on Pt/YSZ (22) this can provide an explanation for the observed quasi-linear increase in E with decreasing $e\Phi$ (Fig. 12).

Reaction Kinetics and Work Function

In order to rationalize the effect of catalyst potential and work function on the reaction kinetics, it is important to discuss the observed sharp maximum of the reaction rate with respect to $P_{C_3H_6}$ (Fig. 4). This maximum and the consequent dramatic rate decrease is due to the surface reaction inhibition from the strong adsorption of propylene (32). When $P_{C_3H_6}$ exceeds a critical value ($P^*_{C_3H_6}$) (Fig. 4), propylene adsorption inhibits the surface reaction. The fact that above $P^*_{C_3H_6}$ the surface species coverages change significantly is manifest in Fig. 14. From this figure it becomes apparent that above $P^*_{C_3H_6}$ the open-circuit catalyst potential, V^o_{WR}, and consequently $e\Phi$, decreases dramatically. This decrease in $e\Phi$ by 0.4 eV shows that when the propylene partial pressure exceeds $P^*_{C_3H_6}$ propylene adsorption dominates and inhibits the surface reaction (32).

The fact that the rate is enhanced via negative potential application in the region of propylene inhibition can be attributed to a strengthening in the chemisorptive bond of electron acceptor oxygen relative to the chemisorptive bond of propylene.

The absence of a promotional effect upon electrochemical O^{2-} supply to the catalyst surface, at least under the conditions investigated in the present work, may reflect the stronger chemisorptive propensity of propylene versus oxygen on the Pt surface as also manifested by the reaction kinetics. Indeed TPD studies of oxygen on Pt under electrochemical O^{2-} supply conditions (27) have shown that strongly bonded promoting anionic oxygen forms on the Pt surface only after the latter is essentially saturated with normally adsorbed atomic oxygen (27). When the surface is not saturated, then electrochemical O^{2-} supply leads to the formation of normally adsorbed oxygen until saturation is reached. Under such conditions one can expect only a Faradaic enhancement in the rate ($I/2F$) if all electrochemically supplied O^{2-} reacts with adsorbed propylene to form CO_2 and H_2O. Such a small rate enhancement would be below the detection limit of the present analytical system.

The above idea is further corroborated by the high operating temperature of the present investigation. Most of the electrochemical pumping experiments were carried out at temperatures above 430°C, i.e. 703 K, where on the basis of TPD work (27) the coverage of atomic oxygen is expected to be well below saturation. This is despite the observed rate plateau at high P_{O_2} values in the present work (Fig. 9). This plateau may reflect a maximum allowable oxygen coverage under conditions of propylene coadsorption.

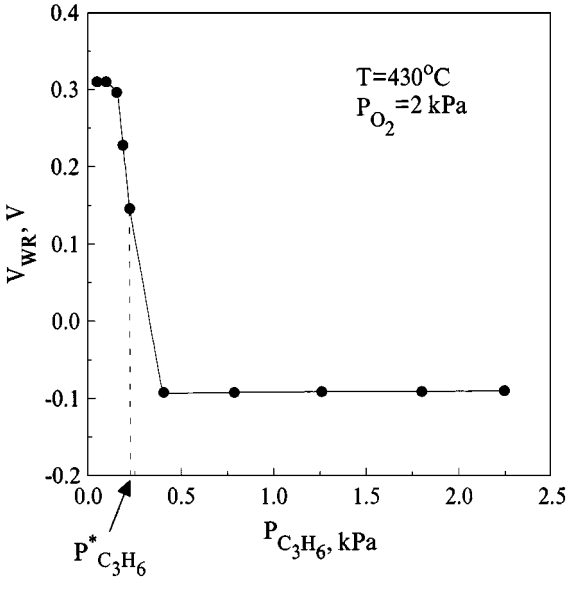

FIG. 14. Effect of $P_{C_3H_6}$ on the catalyst potential, V_{WR}, under open-circuit (o.c.) conditions.

CONCLUSIONS

Propylene oxidation on Pt films deposited on YSZ exhibits a rather strong electrochemical promotion effect at temperatures 400 to 460°C. Negative applied potentials enhance the rate of oxidation by up to a factor of 6. The rate increase is typically a factor of 2000 higher than the rate of electrochemical oxygen removal. Positive potentials application does not affect the reaction rate. The reaction kinetics and apparent activation energy are also significantly modified by the applied negative potentials leading to the appearance of the compensation effect. These kinetic modifications and the observed pronounced rate enhancement are consistent with the notion that decreasing catalyst potential and work function enhances the chemisorptive bond stength of oxygen, relative to dissociative propylene chemisorption on the Pt surface. The high chemisorptive bond strength of propylene appears to be the reason for both the observed reaction rate inhibition and for the absence of a promotional effect at positive potentials.

ACKNOWLEDGMENTS

Sincerest thanks are expressed to DuPont and also to the PENED Programme of the Hellenic Secretariat of Research and Technology for partial financial support.

REFERENCES

1. Vayenas, C. G., Bebelis, S., and Neophytides, S., *J. Phys. Chem*. **92**, 5083 (1988).
2. Bebelis, S., and Vayenas, C. G., *J. Catal*. **118**, 125 (1989).

3. Vayenas, C. G., Bebelis, S., and Ladas, S., *Nature (London)* **343**, 625 (1990).
4. Pritchard, *Nature (London)* **343**, 592 (1990).
5. Yentekakis, I. V., Moggridge, G., Vayenas, C. G., and Lambert, R. M., *J. Catal.* **146**, 293 (1994).
6. Vayenas, C. G., Bebelis, S., and Despotopoulou, M., *J. Catal.* **128**, 415 (1991).
7. Politova, T. I., Sobyanin, V. A., and Belyaev, V. D., *React. Kinet. Catal. Lett.* **41**, 321 (1990).
8. Makri, M., Buekenhoudt, A., Luyten, J., and Vayenas, C. G., *Ionics* **2**, 282 (1996).
9. Tsiplakides, D., Neophytides, S., Enea, O., Jaksic, M. M., and Vayenas, C. G., *J. Electrochem. Soc.* **144**(6), 2072 (1997).
10. Yentekakis, I. V., and Vayenas, C. G., *J. Catal.* **149**, 238 (1994).
11. Pliangos, C., Yentekakis, I. V., Ladas, S., and Vayenas, C. G., *J. Catal.* **159**, 189 (1996).
12. Neophytides, S., Tsiplakides, D., Stonehart, P., Jaksic, M. M., and Vayenas, C. G., *Nature (London)* **370**, 45 (1994).
13. Neophytides, S. G., Tsiplakides, D., Stonehart, P., Jaksic, M. M., and Vayenas, C. G., *J. Phys. Chem.* **100**, 14803 (1996).
14. Anastasievic, N., and Werner, D., "Proc. GDCh Angew. Electrochem., Monheim, October 1996," Vol. 9, p. 27.
15. Vayenas, C. G., Bebelis, S., Yentekakis, I. V., and Lintz, H.-G., *Catal. Today* **11**, 303 (1992).
16. Vayenas, C. G., Jaksic, M. M., Bebelis, S., and Neophytides, S. G., *in* "Modern Aspects of Electrochemistry" (J. O. 'M. Bockris, B. E. Conway, and R. E. White, Eds.), Vol. 29, p. 57. Plenum Press, New York, 1995.
17. Vayenas, C. G., and Neophytides, S. G., *in* "Catalysis, Vol. 12, Chap. 6, p. 199." The Royal Society of Chemistry, Cambridge, 1996.
18. Varkaraki, E., Nicole, E., Plattner, E., Comninellis, Ch., and Vayenas, C. G., *J. Appl. Electrochem.* **25**, 978 (1995).
19. Pliangos, C., Yentekakis, I. V., Verykios, X. E., and Vayenas, C. G., *J. Catal.* **154**, 124 (1995).
20. Marina, O., Yentekakis, I. V., Vayenas, C. G., Palermo, A., and Lambert, R. M., *J. Catal.* **166**, 218 (1997).
21. Ladas, S., Kennou, S., Bebelis, S., and Vayenas, C. G., *J. Phys. Chem.* **97**, 8845 (1993).
22. Kaloyannis, A., and Vayenas, C. G., *J. Catal.* **171**, 148 (1997).
23. Palermo, A., Tikhov, M. S., Filkin, N., Lambert, R. M., Yentekakis, I. V., and Vayenas, C. G., *Stud. Surf. Sci. Catal.* **101**, 513 (1996).
24. Arakawa, T., Saito, A., and Shiokawa, J., *Chem. Phys. Lett.* **94**, 250 (1983). [Appl. Surf. Sci. **16** 365 (1983)]
25. Basini, L., Cavalca, C. A., and Haller, G. L., *J. Phys. Chem.* **88**, 10853 (1994).
26. Kondarides, D. I., Papatheodorou, G. N., Vayenas, C. G., and Verykios, X. E., *Ber. Bunsenges. Phys. Chem.* **97**, 709 (1993).
27. Neophytides, S., and Vayenas, C. G., *J. Phys. Chem.* **99**, 17063 (1995).
28. Makri, M., Vayenas, C. G., Bebelis, S., Besocke, K., and Cavalca, C. A., *Surf. Sci.* **369**, 351 (1996).
29. Ladas, S., Bebelis, S., and Vayenas, C. G., *Surf. Sci.* **251/252**, 1062 (1991).
30. Zipprich, W., Wiemhofer, H.-D., Vohrer, U., and Gopel, W., *Ber. Bunsengesel. Phys. Chem.* **99**, 1406 (1995).
31. Pacchioni, G., Ilas, F., Neophytites, S., and Vayenas, C. G., *J. Phys. Chem.* **100**, 16653 (1996).
32. Hirofumi, S., Hideaki, M., and Yoshiyasu, F., *Appl. Catal.* **49**, 195 (1989).
33. Patterson, W. R., and Kemball, L. L., *J. Catal.* **2**, 465 (1963).
34. Schwaltz, A., Holbrook, L. L., and Prestridge, *J. Catal.* **57**, 41 (1979).
35. Voltz, S. E., Morgan, C. R., Liederman, D., and Jacob, S., *Ind. Eng. Chem., Prod. Res. Dev.* **12**, 294 (1973).
36. Yu Yao, Y. F., *Ind. Eng. Chem., Prod. Res. Dev.* **19**, 293 (1980).
37. Yu Yao, Y. F., *J. Catal.* **87**, 152 (1984).
38. Kim, Y., Shi, S.-K., and White, J. H., *J. Catal.* **61**, 374 (1980).
39. Ueda, W., Asakawa, K., Chen, C.-L., Moro-oka, Y., and Ikawa, T., *J. Catal.* **101**, 360 (1986).
40. Monnier, J. R., and Keulks, G. W., *J. Catal.* **68**, 51 (1981).
41. Keulks, G. W., Yu, Z., and Krenzke, L. D., *J. Catal.* **84**, 38 (1983).
42. Krenzke, L. D., and Keulks, G. W., *J. Catal.* **61**, 316 (1980).
43. Muradyan, A. A., Gazaryan, K. G., Garibyan, T. A., and Nalbadyan, A. B., *Kinet. Catal.* **83/2401**, 93 (1983).
44. Muradyan, A. A., Gazaryan, K. G., Garibyan, T. A., and Nalbadyan, A. B., *Kinet. Catal.* **84/2506**, 1213 (1985).
45. Salmeron, M., and Somorjai, G. A., *J. Phys. Chem.* **86**, 341 (1982).
46. Anderson, A. B., Kang, D. B., and Kim, Y., *J. Am. Chem. Soc.* **106**, 6597 (1984).
47. Kaloyannis, A. C., Pliangos, C. A., Yantekakis, I. V., and Vayenas, C. G., *Ionics* **1**, 159 (1995).
48. Yentekakis, I. V., and Bebelis, S., *J. Catal.* **137**, 278 (1992).
49. Cavalca, C. A., Larsen, G., Vayenas, C. G., and Haller, G. L., *J. Phys. Chem.* **97**, 6115 (1993).
50. Karavassilis, Ch., Bebelis, S., and Vayenas, C. G., *J. Catal.* **160**, 205 (1996). [**160**, 190 (1996)]
51. Cremer, E., *Adv. Catal.* **7**, 75 (1955).
52. Schwab, G.-M., *J. Catal.* **84**, 1 (1983).